NINTH EUROPEAN ROTORCRAFT FORUM

Paper No. A

TESTING AND EVALUATION OF A STALL FLUTTER SUPPRESSION SYSTEM FOR HELICOPTER ROTORS USING INDIVIDUAL BLADE CONTROL

Todd R. Quackenbush

September 13 - 15, 1983
STRESA - ITALY

Associazione Italiana di Aeronautica ed Astronautica
Associazione Industrie Aerospaziali

TESTING AND EVALUATION OF A STALL FLUTTER SUPPRESSION SYSTEM FOR HELICOPTER ROTORS USING INDIVIDUAL BLADE CONTROL

by

TODD R. QUACKENBUSH*

ABSTRACT

The development and testing of a feedback system designed to alleviate the violent blade first torsion mode oscillations associated with stall flutter are described. The system, based on previously developed M.I.T. Individual-Blade-Control hardware, employs blade-mounted sensors to detect torsional oscillations and provide feedback to increase the damping of the first torsional mode. A model of the blade and control system dynamics is developed and is used to give qualitative and quantitative quidance in the design process as well as to aid in analysis of experimental results. System performance in wind tunnel tests, both in hover and forward flight, is described, and experimental results show that the system can provide substantial additional damping to stall-induced oscillations.

*Ph.D. Candidate at Princeton University in the Department of Mechanical and Aerospace Engineering.

NOMENCLATURE

D	motor viscous friction constant, n-m-sec
D_A	aerodynamic damping constant
G_{oL}	open loop transfer function
I	motor current, amps
J_B	blade pitching inertia
J_T	inertia of motor, tachometer and linkage
K_E	volts back EMF, volt-sec
K_F	control system feedback gain
K_{NR}	non-rotating torsional spring constant
K_P	feedback potentiometer gain
K_T	torque sensitivity of motor, n-m/amp
K_{θ}	pitch angle feedback gain
$K_{\dot{\theta}}$	tachometer feedback gain
L_a	motor inductance, ohm-sec
$P_{(\ )}$	system poles
R	motor resistance, ohms
V	voltage input to motor
θ_c	blade pitch angle command
θ_o	collective pitch
θ_1	cyclic pitch
ω_θ	blade first torsion frequency

1. Introduction

As increased demands on helicopter performance have pushed machines to higher values of blade loading and advance ratio, one persistent problem for the designer has been the aeroelastic instability known as stall flutter. This phenomenon has been extensively studied in a variety of other works (Refs. 1-4, for example) and a comprehensive discussion of its sources and effects is not necessary for present purposes. However, a brief summary of the salient points is helpful for posing the design problem dealt with herein.

It has been well documented that an airfoil oscillating rapidly in pitch is able to operate transiently at angles of attack considerably in excess of its static stall angle without flow separation taking place. However, at sufficiently high angles of attack, the airfoil stalls, though this so-called dynamic stall differs considerably from conventional static airfoil stall. As shown by Ham, Ref. 4, dynamic stall is characterized by the loss of leading edge suction and the subsequent movement of a large negative pressure disturbance aft from the leading edge, a movement which generates strong nose-down pitching moments on the airfoil. With proper combinations of airfoil mean angle of attack, amplitude of motion, and reduced frequency, this stalling phenomenon can cause hysteresis in the aerodynamic pitching moment which can lead to a net influx of energy to the airfoil's pitching motion.

The application of these findings for airfoil dynamic stall to helicopter rotor blades is relatively straightforward. Figure 1 shows a typical azimuthal angle of attack distribution for a rotor blade in forward flight. The high angles of attack on the retreating side and the rapid angle of attack variations caused by the blade motion strongly suggest that rotor blades under certain conditions should be susceptible to the same stall-induced oscillations observed in airfoils. Both experiments and flight experience has shown that this is indeed the case; for certain combinations of torsional natural frequency, blade loading, and advance ratio, the spanwise integrated effect of dynamic stall is to feed energy into blade torsional motion, particularly the first torsion mode. The resulting motion is generally only unstable over part of the azimuth and damps out rapidly as the blade swings around toward the advancing side. However, even the one or two cycles of large amplitude torsional motion that do occur are sufficient to put extreme loads on the rotor control system (see Fig. 2); the fatigue life of rotor pitch links can thereby be considerably reduced.

The adverse effects of stall flutter could, of course, be alleviated by such expedients as increasing solidity. However, such a change would increase the drag of the rotor and would penalize the performance of the helicopter at all speeds. Also the development of airfoils with more benign dynamic stall characteristics may be possible, but attempts to identify such airfoils have so far been inconclusive (e.g., Ref. 5).

Applying Individual-Blade-Control (IBC) techniques to this problem offers a possible solution. Reference 6 showed that appropriate feedbacks to a position control servo governing blade pitch motion could help reduce undesirable blade motions due to low-frequency gust inputs. It was felt that similar methods could be applied to alleviate the violent torsional motions associated with stall flutter. To understand the overall concept that was employed, consider again for a moment the mechanism which drives the stall flutter oscillations. As noted previously at high blade angles of attack and certain reduced frequencies, aerodynamic moment hysteresis causes a net input of energy to blade torsional motion, so that any small blade oscillation grows with time. Such a situation is equivalent to a one-degree-of-freedom oscillating system with negative damping. Indeed, stall flutter can be conceived of as a phenomenon caused by a once per revolution variation in the effective damping of the blade in pitch. On the advancing side, the blade experiences positive damping at low angles of attack; but on the retreating side the effective damping can temporarily become negative, leading to the self-limiting oscillations described above. Figure 3 gives an idea of the variation of the effective damping function with blade operating condition.

An effective stall flutter suppression system, then, would be one which could eliminate this one-per-rev excursion into negative damping. One way to achieve this end which is suggested by classical control theory is to provide a pitch rate feedback from the blade to the pitch control servo. The details of the rationale for this concept, its implementation, and the results of experiments based on it are given in the following sections.

2. An Idealized Stall Flutter Suppression System

The Individual Blade Control concept postulates that the pitch of each rotor blade will be controlled individually by the action of electro-mechanical or electrohydraulic actuators. It thus provides a natural framework for feedback control of the rotor blades. To see how this general design concept was applied to stall flutter suppression, consider the diagram of an idealized IBC system, given in Fig. 4. As suggested in the previous section, a pitch rate feedback to the actuator control appeared to be an appropriate choice to bring about additional damping of the blade's stall-induced torsional oscillations. Such a pitch rate signal could be extracted by mounting appropriately oriented accelerometers on the blade to sense the onset of stall flutter oscillations. The acceleration signal could then be integrated and an appropriate gain applied to provide the desired weighted feedback.

The plausibility of the rate feedback approach is indicated by the simple root locus diagram in Fig. 4. The blade dynamics are represented there by poles residing near the imaginary axis; the effect of the stall-induced negative aerodynamic damping is, essentially, to push these poles into the right half-plane for some fraction of the rotor rotation period. Using rate feedback to place a zero at the origin and applying a nonzero

feedback gain, the damping of the blade oscillation will increase; for this simple model, any desired level of positive damping can be applied.

Clearly, the inclusion of actuator dynamics alters this simplified presentation. In such a case the pole trajectories given in Fig. 4 are substantially changed, even if aerodynamic effects are neglected. Also, it is obvious that, in a rigorous sense, root locus analysis is not applicable to this problem because of the highly nonlinear aerodynamic effects associated with the stall flutter. Despite these caveats, however, the following discussion will show that simple models and analysis methods such as root locus techniques serve as very useful points of departure for the design of an effective flutter suppression system.

3. Mechanization of the Control System

The model used here to test the proposed stall flutter suppression system was identical in most particulars to that used in Ref. 6. A D.C. servomotor acting, through a series of linkages, as a blade pitch position control system was mounted on the rotor shaft. The test rotor used only a single blade, with a NACA 0012 section, 21.2 inch span, and a two inch chord; further details on the blade are given in Table 1. A steel flexure instrumented with strain gauges was attached to the blade to sense pitch angle.

Two "dummy blades" in the form of lengths of threaded 5/8" steel rod were also attached to the rotor hub. Each rod had adjustable counterweights which were used to achieve dynamic balancing during rotor operation. Two symmetrically mounted counterweights were also attached to the shaft to balance the mass moment of inertia contribution of the active rotor.

Since the primary aim of this experiment was to design a system to control the first torsion mode of the rotor, it was necessary to insure that the frequency of the mode was within the bandwidth of the servomotor. For full scale rotor blades, ω_θ is usually to the order of 5Ω to 7Ω, or about 30-40 Hz for most helicopters. Unfortunately, values of ω_θ for small, relatively stiff model blades such as the one employed here are invariably much higher than for full scale blades; in this case, it would have been very difficult, because of the high values of ω_θ in the test blade, to induce the blade itself to flutter. Given this, it was necessary to introduce additional "softness" into the blade artificially. Two leaves of spring steel were therefore inserted between the actuator control fork and blade itself. The first torsion frequency of this modified blade was 31.8 Hz.

The pitch acceleration signal required for the feedback system was extracted using the accelerometer configuration shown in Ref. 7. Only two accelerometers were available for these experiments; with these, the "propeller moment" due to centrifugal effects could be eliminated but some cyclic and flapping effects could not. As will be seen, this circumstance tends to obscure some of the results obtained but does not adversely affect

the overall performance of the system.

Photographs at the blade and control system hardware are shown in Ref. 7. Further details of the construction of the actuation system are given in Ref. 6 and will not be repeated here.

4. Analysis of Control System

The principal aims of the analysis carried out for this design were to ascertain the probable performance limits of the system in terms of providing increased damping to the blade's torsional motion and to make an estimate of the feedback gain required to obtain substantial beneficial effects. The starting point for this analysis was the derivation of the servo motor transfer function from the system equations of motion:

$$\dot{I}\, L_a + IR + K_E\, \dot{\theta}_c = V \tag{1}$$

$$-K_T I + J_T\, \ddot{\theta}_c + D\dot{\theta}_c + \frac{K_{NR}}{2}\left(\frac{\theta_c}{2} - \theta\right) = 0 \tag{2}$$

$$J_B \ddot{\theta} + K_{NR}\,(\theta - \theta_c/2) = 0 \tag{3}$$

Using these equations, the servo transfer function becomes

$$\frac{\dot{\theta}_c}{I} = \frac{5000\left(\frac{S^2}{(194.7)^2} + 1\right)}{\left(\frac{S}{.366} + 1\right)\left(1 - \frac{S}{p_1}\right)\left(1 - \frac{S}{\bar{p}_1}\right)} \tag{4}$$

$$p_1 = -.057 + 220.1j$$

As shown in Fig. 5, tachometer and angle feedbacks were run to the servo input to form a position control system. Through a 2:1 reduction gear, this system controlled the pitch of the blade. For the values of K_θ and $K_{\dot{\theta}}$ shown in Fig. 5, the pitch actuator transfer function was,

$$\frac{\theta_c}{V} = \frac{(.131)\left(\frac{S^2}{(194.7)^2} + 1\right)}{\left(\frac{S}{1227.0} + 1\right)\left(\frac{S}{160.6} + 1\right)\left(1 - \frac{S}{p_2}\right)\left(1 - \frac{S}{\bar{p}_2}\right)} \tag{5}$$

$$p_2 = -2.75 + 192.9j$$

For the purposes of the preliminary analysis, the effects of aerodynamics in the blade dynamics were neglected, so the open loop transfer

function of the system became,

$$G_{oL} = \frac{.127\ K_F\ S^3}{(\frac{S}{160.6} + 1)(\frac{S}{1227.0} + 1)(1 - \frac{S}{p_2})(1 - \frac{S}{\bar{p}_2})(1 + \frac{S}{3.0})^2} \tag{6}$$

The root locus in this system is shown in Fig. 6. The locus is very different from the idealized sketch of Fig. 4, because of the presence of the two actuator poles on the real axis; however, the application of feedback still leads to substantially increased damping of the blade oscillations. The two values of feedback potentiometer setting, K_p, that are marked on the locus represented what was felt to be a reasonable increment of damping for design purposes (the given increment in K_p yields an increase in ζ from .014 to .09).

To obtain a first approximation of the effects of negative aerodynamic damping on this system, a constant term $D_A\dot{\theta}$ was inserted into the equations of motion, Eqs. (1-3). The value of D_A was chosen to yield an effective damping ratio of -0.1 for the blade's torsional motion. This constant D_A corresponds to having the negative damping associated with stall flutter persist all around the azimuth. For this case, the transfer function of the position control system becomes,

$$\frac{\theta_c}{V} = \frac{.131\ (\frac{S^2}{(194.7)^2} + \frac{2(-0.1)}{(194.7)}S + 1)}{(\frac{S}{160.0} + 1)(\frac{S}{1207.1} + 1)(1 - \frac{S}{p_3})(1 - \frac{S}{\bar{p}_3})} \tag{7}$$

$$p_3 = +16.9 + 192.3j$$

The dynamics of the system do not change dramatically, except that the branch of the locus describing the blade motion shifts toward the right half-plane. As Fig. 6 shows, though, even this rather severe instability could be stablized given a properly chosen feedback gain.

Obviously simple root locus techniques do not model many aspects of the blade's dynamic behavior with complete accuracy. More sophisticated analysis methods could be brought to bear on this problem if desired. For example, describing functions could be used to develop a model incorporating the aerodynamic moment hysteresis associated with stall flutter to replace the simple blade model used here. However, the approach already described yielded satisfactory guidance for the proof-of-concept experiments to be run here, so such additional complexities were deemed unnecessary.

5. Experimental Results

Testing of the I.B.C. stall flutter suppression system was performed in the 7' x 10' Wright Brothers Wind Tunnel at M.I.T. The model rotor was driven by an external hydraulic motor. The shaft was equipped with slip rings to provide power to the servo-motor and to extract data from the various sensors. On-line data extraction was accomplished using a PDP-11 computer and software previously developed by other members of the I.B.C. project team.

The major results of the testing series are contained in three sets of experiments. First, a set of non-rotating cases were run, both closed and open loop, to test the performance of the system in an undemanding, easily controlled environment. The second group was a set of forward flight tests at moderate advance ratio ($\mu = 0.30$) featuring a mild excitation of stall flutter. Finally, a third group of experiments was run at a slightly higher advance ratio ($\mu = 0.33$) where very vigorous stall flutter excitation was present in the open-loop case.

For the first set of non-rotating runs, the blade motion was excited by applying a pulse train to the input of the pitch actuator (the pulses had a duration of 4.0 ms., a frequency of 6.0 Hz and an amplitude of 0.75 volts, equivalent to 3° of pitch). The response of the blade is shown in Fig. 7. The open loop torsional oscillation is very lightly damped ($\zeta = 0.03$). However, closing the loop and applying feedback potentiometer settings of $K_p = 0.13$ and 0.26 yields the results shown in Figs. 8 and 9; the damping of the blade motion has been significantly increased, reaching $\zeta \cong 0.3$ for the $K_p = 0.26$ case. Figure 10 gives additional insight into the system's performance, showing that the component of the blade motion at the first torsion frequency is decreased by almost 90% relative to the open loop case, with $K_p = .26$.

It is also worth noting that the frequency of oscillation increases somewhat with the application of feedback. This trend was predicted in the root locus diagram of Fig. 6. However, the damping ratio achieved in the closed loop tests is considerably larger than that shown in Fig. 6. This suggests that more damping was present in the system than the linear model could account for (a probable source is Coulomb damping associated with gear meshing and the flexing of the torsional spring at the root).

The forward flight tests consisted of two sets of runs, the first with a $\Omega = 6.7$ Hz and the second with $\Omega = 6.1$ Hz. Since the wind speed in each case was 29 fps, the advance ratios were 0.30 and 0.33, respectively. In the first case, a relatively mild excitation of stall flutter was observed in the open loop case (Fig. 11) ($\theta_o = 16°$, $\theta_1 = \pm 8°$). Note again that the low frequency component dominating the time traces for the forward flight runs represents the cyclic input; the torsional oscillations due to stall flutter appear as the small, high frequency peaks superposed on these waveforms.

The application of a moderate level of feedback gain (K_p = 0.13) produced a noticeable increase in the damping of the stall-induced oscillations. (See Fig. 12.) The time trace of the accelerations smoothed out somewhat and the component of the blade motion at the first torsion frequency dropped by some 40%. Increasing the feedback still further, to K_p = .26, produced more of the same trend; a slightly smoother waveform and a first torsion component down to some 30% of its open loop value (Fig. 13).

Increasing the advance ratio to 0.33 brought about a much more vigorous stall flutter oscillation, as indicated in Fig. 14. However, with the application of the same levels of feedback gain noted above, the situation improved dramatically. Figures 15 and 16 show the marked reductions in blade torsional oscillations brought about by closing the feedback loop. For K_p = 0.26, Fig. 16 indicates that the blade motion at its torsional natural frequency has been reduced to approximately 10% of its original value.

6. Discussion of Results

As the results presented above show, the flutter suppression system designed for this experiment was successful in its basic objective: adding substantial amounts of damping to the torsional motion of a model rotor to compensate for transient, stall-induced negative damping. However, some aspects of the results warrant more discussion, and some comments can be made on the direction that future research in this area might take.

One ostensibly anomalous result can be observed in Fig. 11. Typically, stall flutter oscillations die out rapidly as the blade swings around the azimuth to the advancing side and positive aerodynamic damping is encountered. In Fig. 11, however, some blade oscillations persist well into the advancing side, though they clearly are being damped out. One reason for this behavior is that on "typical" blades, ω_θ is in the vicinity of 7Ω to 8Ω, while here ω_θ is roughly 5Ω. This means that for a given value of damping ratio the model blade used here will require a longer time (in terms of degrees of azimuth covered) for torsional motion to damp out than would a full scale blade. Also, most full size rotor blades are mass balanced, with centers of gravity at or ahead of the quarter chord; this blade has its c.g. at 31% of chord, and Ham in Reference 2 found that for such aft c.g. positions stall-induced oscillations could be made to persist well into the advancing side, as was observed here.

Another issue of concern is the effectiveness of this system in reducing the peak loading experienced by the control system. The results presented so far have amply demonstrated the system's ability to add enough damping to cause stall-induced oscillations to die away relatively rapidly. However, as comparison of Figs. 7 and 9 suggest, the blade acceleration, and hence the peak load on the pitch control mechanism, is decreased only by about

10% by closing the feedback loop. Since, to a reasonable approximation, the first peak height is reduced by a fraction of $1 - e^{-\zeta}$ with the addition of damping, much higher damping ratios are needed to obtain substantial relief from peak loads.

A moderately straightforward alteration of the current system could, it appears, achieve this end. Figure 17 gives a conceptual diagram and a root locus plot of the qualitative aspects of the modified system; as the figure indicates, installing a pure gain in parallel with the feedback integrator would provide a mixed acceleration/rate feedback. Proper choice of the gains involved could place the real axis zeros so that, as illustrated, the blade oscillation would never go unstable. Also, much larger values of damping than possible with the current configuration could be achieved, thereby reducing the maximum load on the blade control system due to dynamic stall. This system thus holds the promise of increased damping while retaining the feedback integrator which helps to smooth out the noisy pitch acceleration signal. Obviously, the side effects of such a configuration would have to be investigated (its effect on steady inputs like cyclic pitch, for example), but such concepts suggest that considerable additional progress would be made in suppressing stall flutter without complicating the design used in these experiments.

7. Conclusions

The principal conclusion to be drawn from these experiments is that despite the complex nature of the aerodynamic effects that bring about stall flutter a relatively simple system has been shown capable of alleviating some of its worst effects. The system is simple in concept in that it is based on the idea of providing a rate feedback to increase the damping of an oscillating system; it is simple in execution because it relies principally on the integrated output of accelerometers, weighted by an appropriate gain, to provide the desired rate feedback.

This is not to say that the extension of the concepts discussed here to full-scale helicopters will be trivial. Since the rotational and blade torsional frequencies used here (6 Hz and 31 Hz, respectively) are in the vicinity of typical full-scale values, a helicopter would have to be equipped with pitch actuators roughly as fast as the one employed here to obtain comparable performance (i.e., τ less than approximately .006 sec.). Also, appropriate sensor installation on (very flexible) helicopter blades will doubtless be more challenging than it was on the model blade used in these experiments. Despite these and other potential problems, though, the results presented above indicate that a stall flutter suppression system based on Individual Blade Control techniques holds substantial promise.

References

1) Tarzanin, F. J., Jr.: "Prediction of Control Loads Due to Blade Stall". Journal of the American Helicopter Society, Vol. 17, No. 2, April 1972.

2) Ham, N. D.: "An Experimental Investigation of Stall Flutter". Journal of the American Helicopter Society, Vol. 7, No. 1, January 1962.

3) Carta, F. O., Commerford, G. L. and Carlson, R. G.: "Determination of Airfoil and Rotor Blade Dynamic Stall Response". Journal of the American Helicopter Society, Vol. 18, No. 2, April 1973.

4) Ham, N. D. and Young, M. I.: "Torsional Oscillation of Helicopter Blades Due to Stall". Journal of the American Helicopter Society, Vol. 3, No. 2, May-June 1966.

5) McCroskey, W. J., et al: "Dynamic Stall on Advanced Airfoil Sections". Journal of the American Helicopter Society, Vol. 26, No. 3, July 1981.

6) McKillip, R. M., Jr.: "The Design, Testing and Evaluation of the MIT Individual Blade Control System As Applied to Gust Alleviation for Helicopters". NASA CR-152352, February 1980.

7) Quackenbush, T. R.: "Testing and Evaluation of a Stall Flutter Suppression System for Helicopter Rotors Using Individual Blade Control". NASA CR-166233, August 1981.

TABLE 1

DESCRIPTION OF THE ROTOR BLADE USED IN WIND TUNNEL TESTS

No. of Blades	1
Radius, w/o Steel Leaves	2.03 ft.
Radius w/ Steel Leaves	2.311 ft.
Chord	2.0 in.
Section	NACA 0012
Lift-Curve Slope	5.73
Drag Coefficient	.012
Rotational Speeds, Forward Flight Cases	6.7 Hz (first test) 6.1 Hz (second test)
Aerodynamic Center	25% chord
Hinge Offset	2.0 in.
Built-in Angle of Twist	8 deg. (linear)

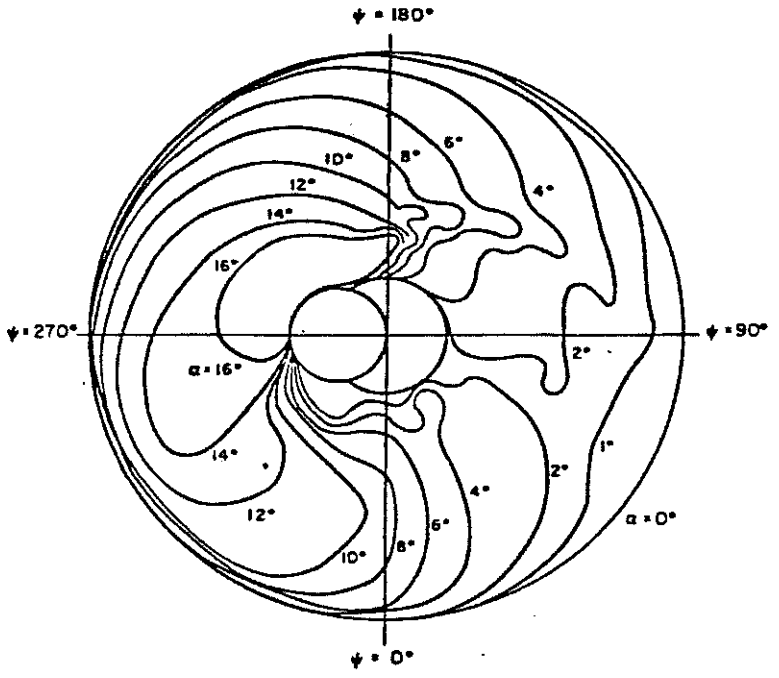

Figure 1. Typical Angle of Attack Distribution for a Rotor in High Speed Forward Flight.

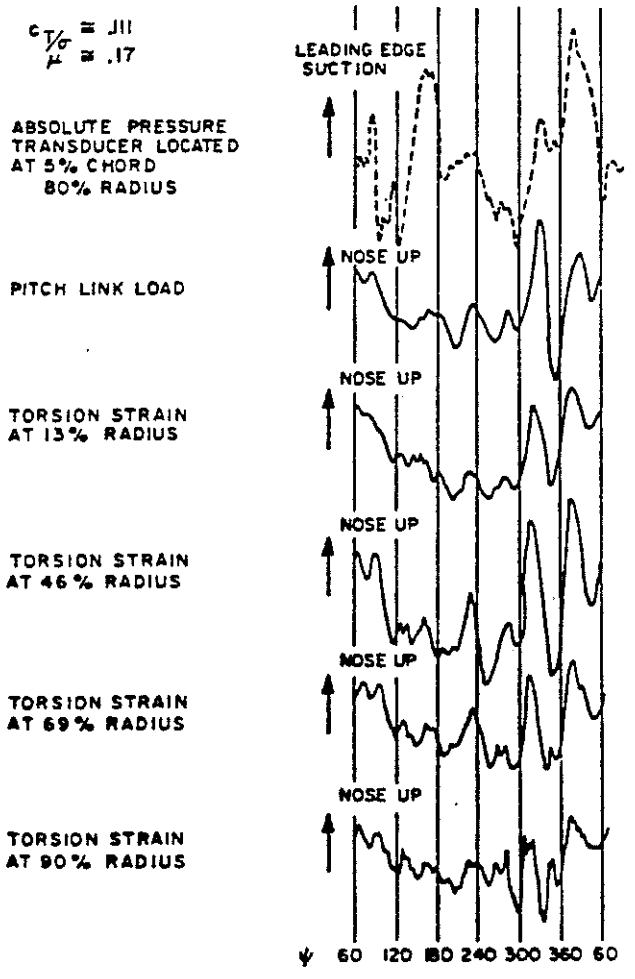

Figure 2. Typical Torsion Loads on a Blade Undergoing Stall Flutter

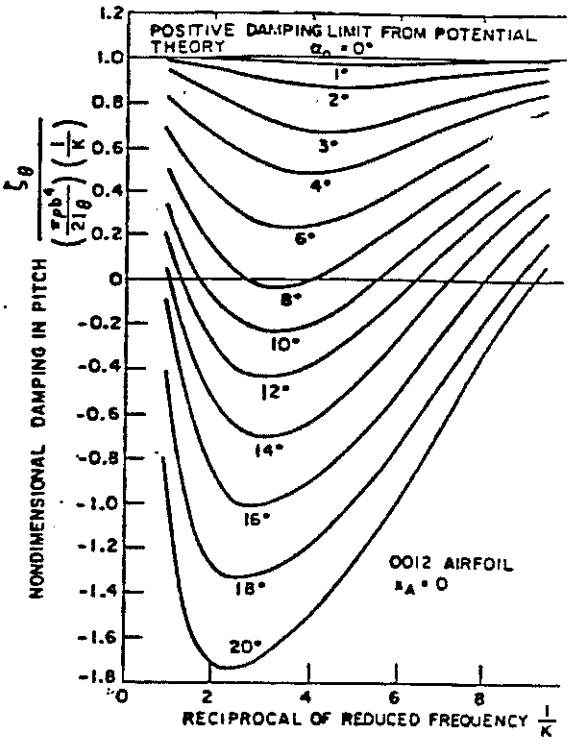

Figure 3. Approximation to Generalized Pitch Damping.

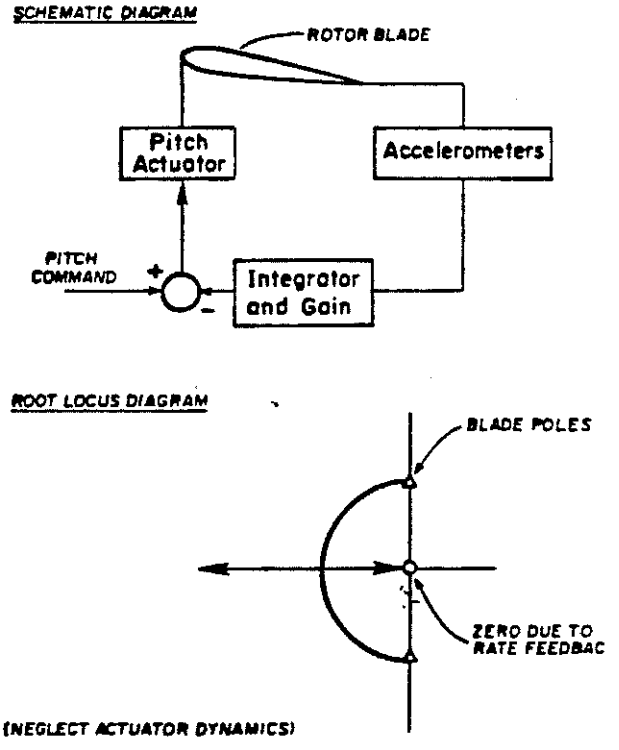

Figure 4. Idealized Stall Flutter Suppression System.

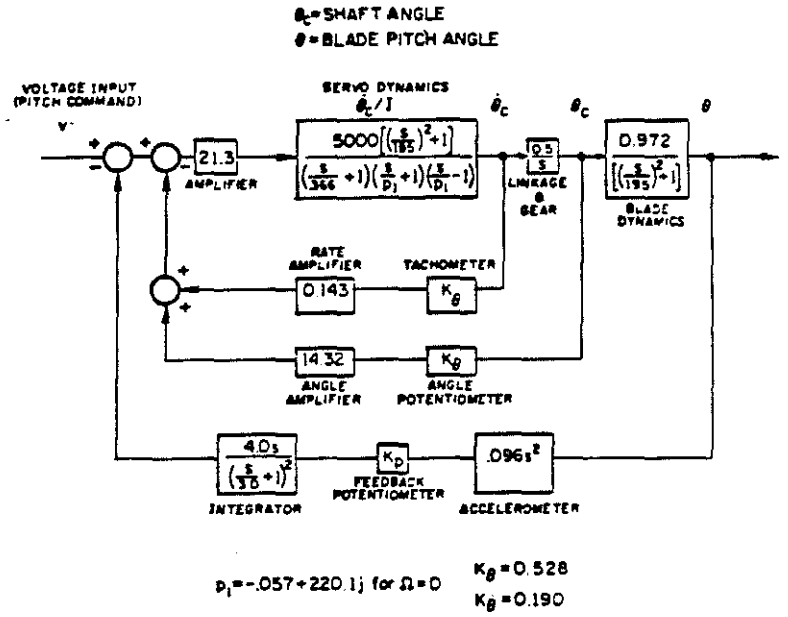

Figure 5. Control System Block Diagram.

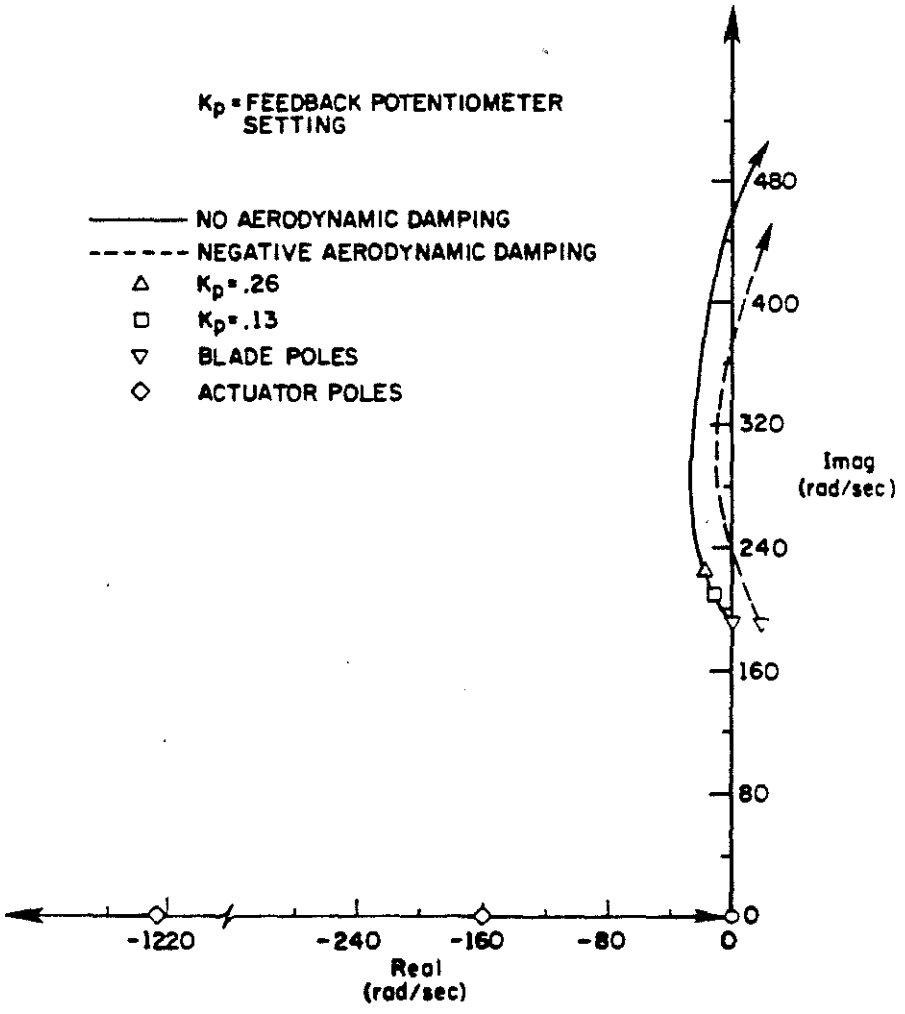

Figure 6. Control System Root Locus (Non-Rotating).

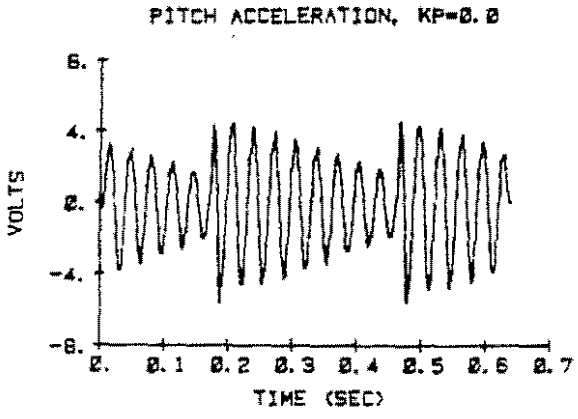

Figure 7. Zero Feedback Response, Non-Rotating Case.

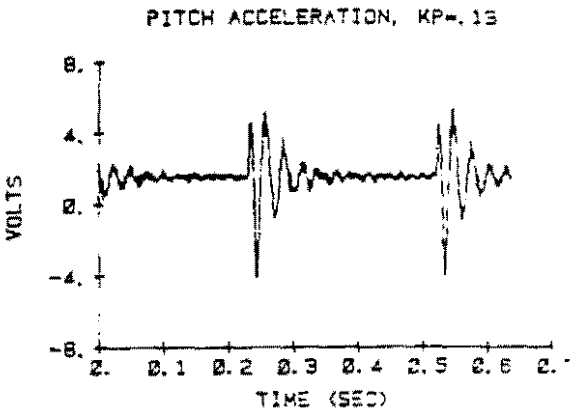

Figure 8. Moderate Feedback Response, Non-Rotating Case.

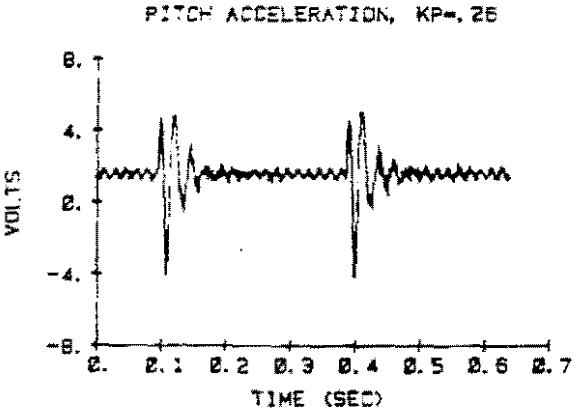

Figure 9. High Feedback Response, Non-Rotating Case.

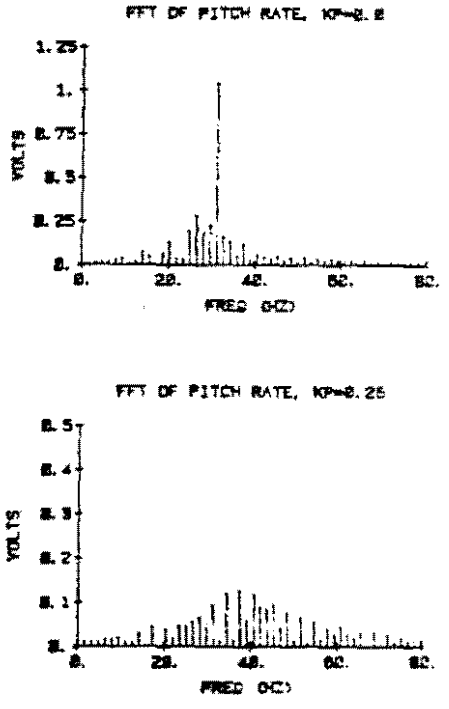

Figure 10. Fourier Transform of Open and Closed Loop Response, Non-Rotating Case

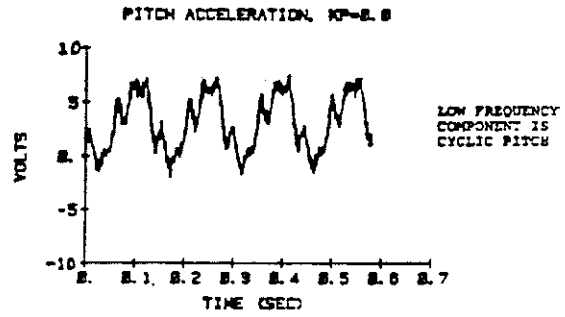

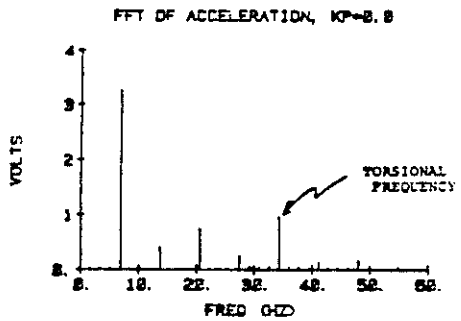

Figure 11. Low Feedback Response, Forward Flight at Advance Ratio of 0.30.

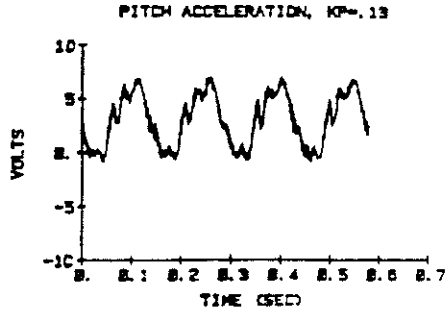

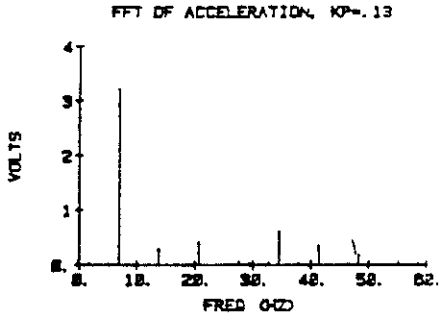

Figure 12. Moderate Feedback Response, Forward Flight at Advance Ratio of 0.30.

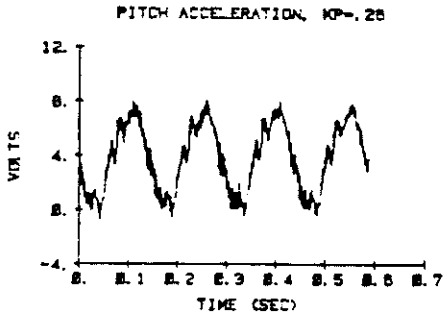

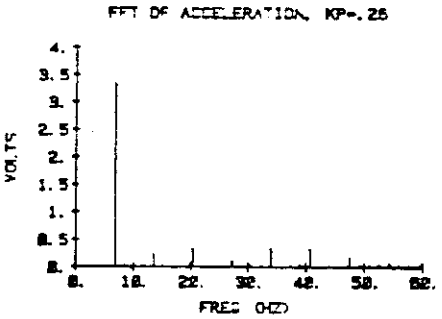

Figure 13. High Feedback Case, Forward Flight at Advance Ratio of 0.30.

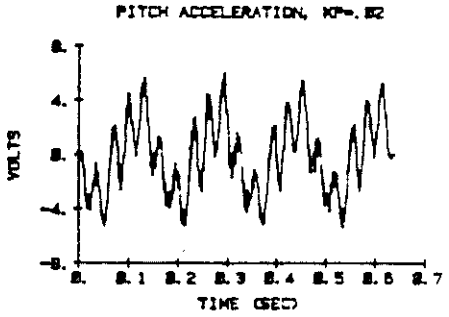

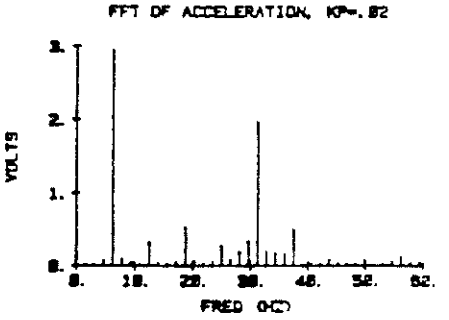

Figure 14. Low Feedback Case, Forward Flight at Advance Ratio of 0.33.

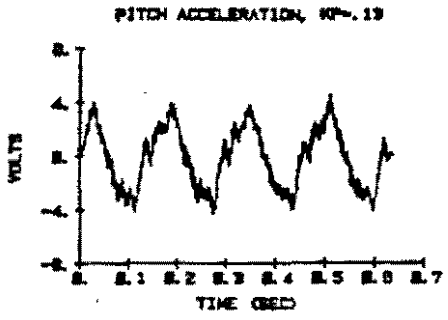

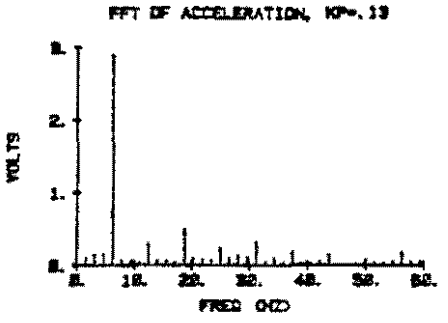

Figure 15. Moderate Feedback Case, Forward Flight at Advance Ratio of 0.33.

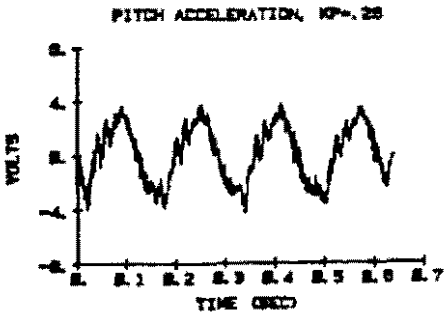

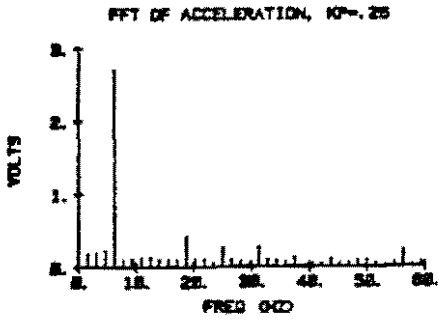

Figure 16. High Feedback Case, Forward Flight at Advance Ratio of 0.33.

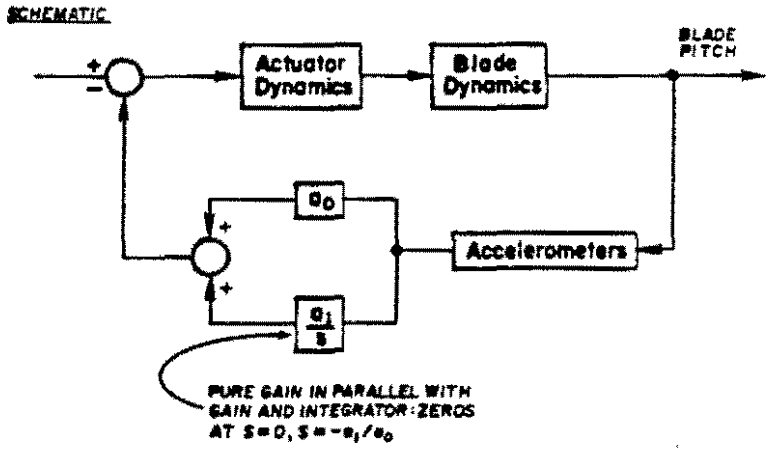

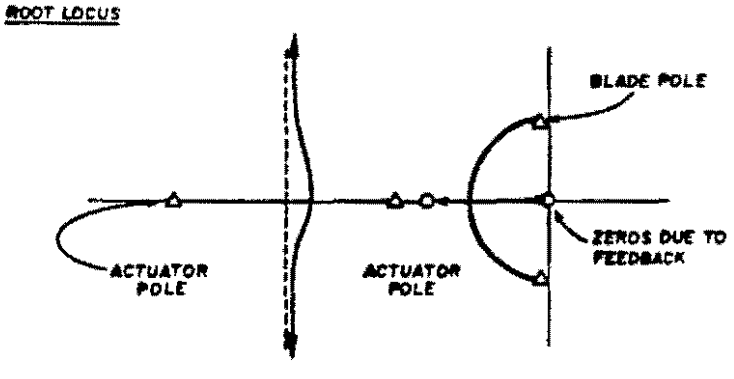

Figure 17. Modified Flutter Suppression System.